PCCP

ARTICLE TYPE

Electronic Supporting Information for: The roto-conformational diffusion tensor as a tool to interpret molecular flexibility

Sergio Rampino,[a] Mirco Zerbetto,*[a] and Antonino Polimeno[a]

[a] *Department of Chemical Sciences, University of Padova, Via Marzolo 1,I-35131, Padova, Italy. Fax: 39 049 8275050; Tel: 39 049 8275678; E-mail: mirco.zerbetto@unipd.it*

Contents

1 Computational details

Calculations were performed starting from local-minimum structures (those sketched in Fig. 1 of the article) and the related Hessian matrix. These were obtained through the Tinker 8 program package[1] using the popular MM3 Force Field (FF)[2–4] (see Refs. 5 and 6 for a review of several FFs for carbohydrates) for **DMF** and the oligosaccharides, and the CHARMM22 FF[7] for **GB3**. Minimization was performed through Tinker's `minimize` tool with a 'RMS Gradient per Atom Criterion' of 0.01 Å. The Hessian matrix was calculated through Tinker's utility `testhess`.

2 Roto-conformational diffusion tensor of the selected oligosaccharides

Figs. 1-5 of the ESI summarize the analysis of the roto-conformational diffusion tensor of the five oligosaccharides **R2R**, **BGL**, **GGM**, **TRI**, and **GCY** that have not been reported in the main text

In addition, we provide a comparative analysis of the results obtained by changing *i*) the physical conditions (temperature, viscosity, hydrodynamic radius), and *ii*) the choice of the triplet of reference atoms used to define the molecule-fixed frame. For these tests we decided to employ the **LNF** molecule, which is made by five sugar units allowing for a complete, but compact analysis of the effect of the choice of the triplet of atoms. In particular, the triplet is chosen to have the ^{13}C-^{1}H NMR probe on C-1 of each of the A-E sugar units (see panel **a** of Fig. 5 of the article for units labeling).

Fig. 6 of the ESI shows results for **LNF** where with respect to the results in the main text, we lowered the temperature from 303.0 K to 253.0 K, and increased the viscosity from 1.4 cP to 28.2 cP according to the properties of the solvent (DMSO-*d*6/D_2O 7:3 molar ratio). Fig. 7 of the ESI shows results for the same system considered in the article with effective radius altered to $R_{\text{eff}} = 2.0$ Å. Figs. 8, 9, 10, and 11 of the ESI show results for the same system considered in the article with the triplet of atoms on sugar units B, C, D and, E, respectively. Tab. 1 of the ESI reports the elements of the diagonal rotational block $\mathbf{D}^{(\text{RR})}$ of the roto-conformational diffusion tensor **D** and the first three eigenvalues of the roto-conformational diffusion tensor **D** for the **LNF** system calculated using the different parameters adopted in the above mentioned Figs. 6 to 11 of the ESI.

The change of the hydrodynamic radius is, at zero-th order, reflected on a scaling of the diffusion tensor (Fig. 6), which is inversely proportional to the radius. Since the diffusion tensor is computed including a hydrodynamic interaction among the atoms [Campeggio, J.; Polimeno, A.; Zerbetto, M. J. Comput. Chem. 2019, 40, 697], the change of the hydrodynamic radius can have higher order contributions, which are not usually relevant in the typical range of 2 - 4 Å. Changing the viscosity at given temperature (i.e., changing the solvent) implies simply a scaling of the diffusion tensor. Changing the temperature/viscosity (Fig. 7), has a different effect on the different blocks of the diffusion tensor. The RR part

scales as T/η, the SS part as T^2/η, and the RS part as $T^{3/2}/\eta$ (because of the transformation to the scaled internal coordinates). Interestingly, reducing the temperature increases the time scale gap between the overall tumbling and the conformational internal motions, which become less correlated. This can be observed by comparing panels d of Fig. 5 of the main text and Fig. 6 of the ESI. In the second plot, the red line shows a lower entity of the coupling between the rotational motion and the internal motion with the highest frequency.
Changing the triplet of atoms defining the orientation frame (Figs. 8-11), instead, has no noticeable effect on the internal part of the scaled roto-conformational diffusion tensor, but results in different values of the elements of the rotational block and, accordingly, of the coupling between the external rotation and the internal motions. In particular, for instance, if the triplet is chosen on a terminal part of the molecule (sugar units A as in Fig. 5 of the main text, or E as in Fig. 11 of the ESI) only one normal scaled coordinate is significantly coupled with the external rotation. However, if the triplet is chosen on an inner part of the molecule (Figs. 8-10), the rotational motionn results coupled to more normal scaled coordinates, but with an overall less intense coupling.

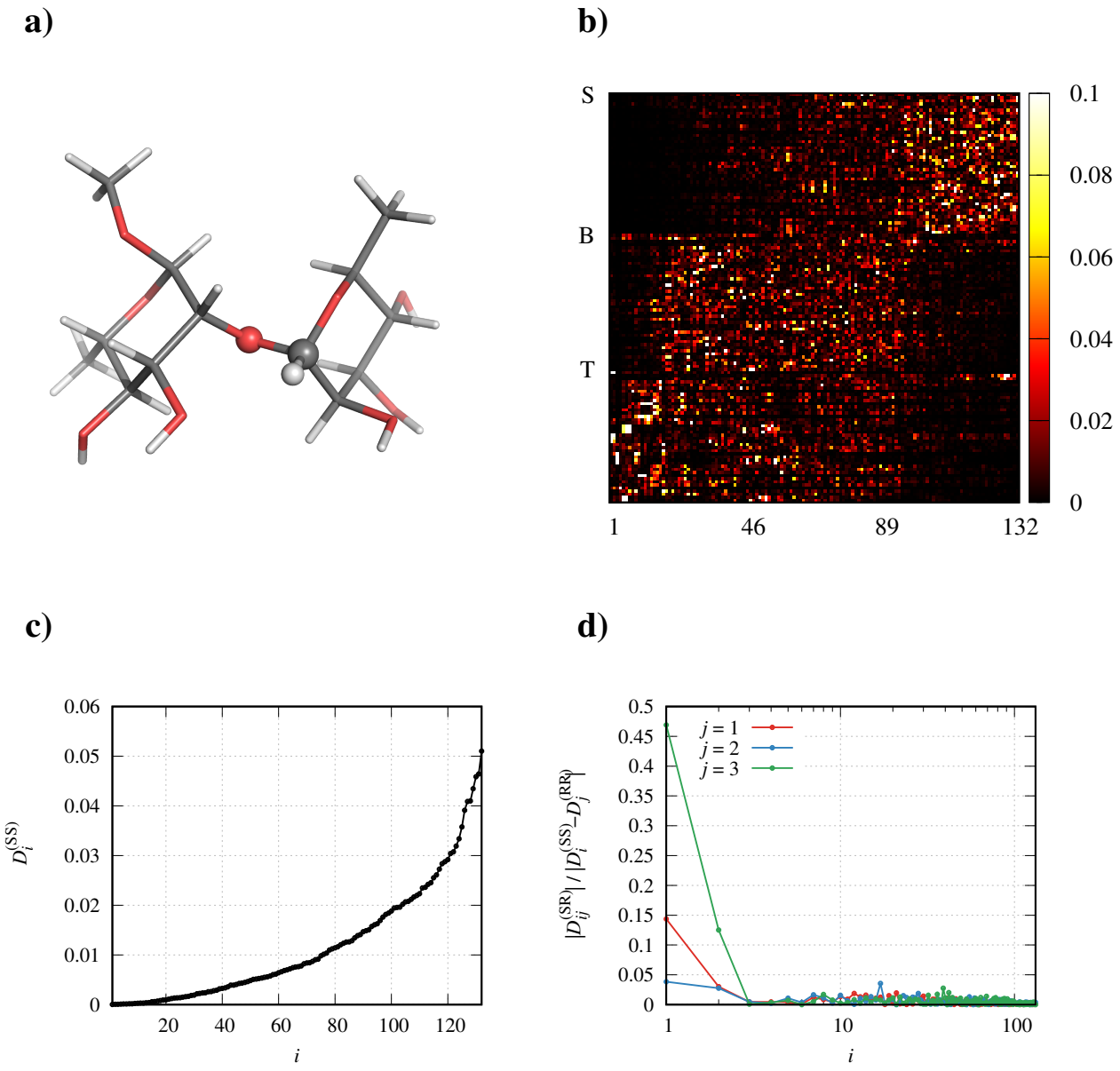

Fig. 1 a) Molecular structure of R2R. b) Color plot of the elements T_{ij}^2 of the matrix diagonalizing the internal block (SS) of the diffusion matrix. The initial row of the stretchings block (rows 1-45), of the bendings block (rows 46-88), and of the torsions block (rows 89-132) is labeled with 'S', 'B', and 'T', respectively. c) Elements $D_i^{(SS)}$ (in fs^{-1}), i.e. eigenvalues of the internal block (SS) of the diffusion matrix. d) Extent of the coupling between the internal motions (each described by the i the normal mode) and the overall rotation (note that the abscissa is in logarithmic scale).

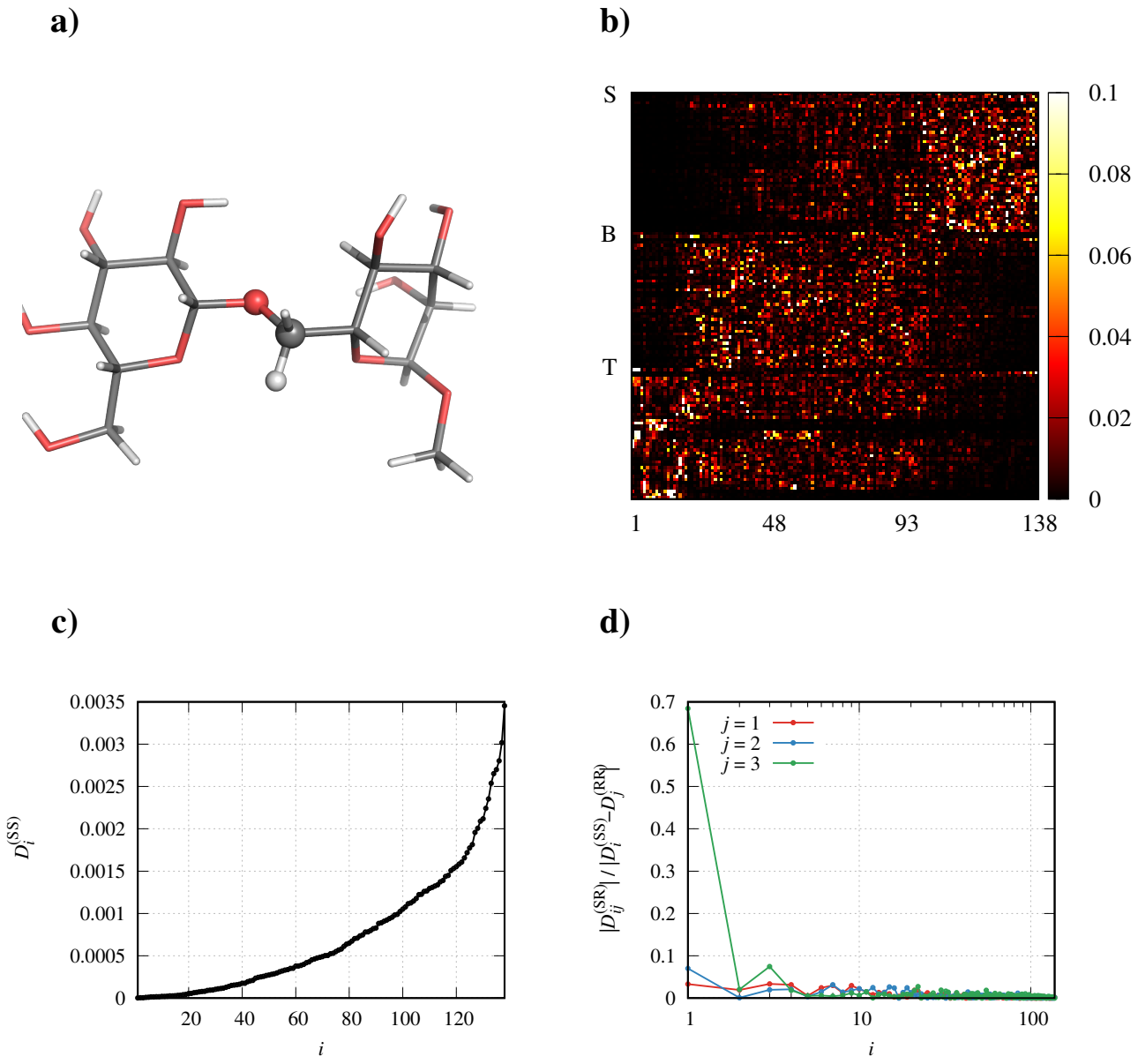

Fig. 2 a) Molecular structure of BGL. b) Color plot of the elements T_{ij}^2 of the matrix diagonalizing the internal block (SS) of the diffusion matrix. The initial row of the stretchings block (rows 1-47), of the bendings block (rows 48-92), and of the torsions block (rows 93-138) is labeled with 'S', 'B', and 'T', respectively. c) Elements $D_i^{(SS)}$ (in fs^{-1}), i.e. eigenvalues of the internal block (SS) of the diffusion matrix. d) Extent of the coupling between the internal motions (each described by the i the normal mode) and the overall rotation (note that the abscissa is in logarithmic scale).

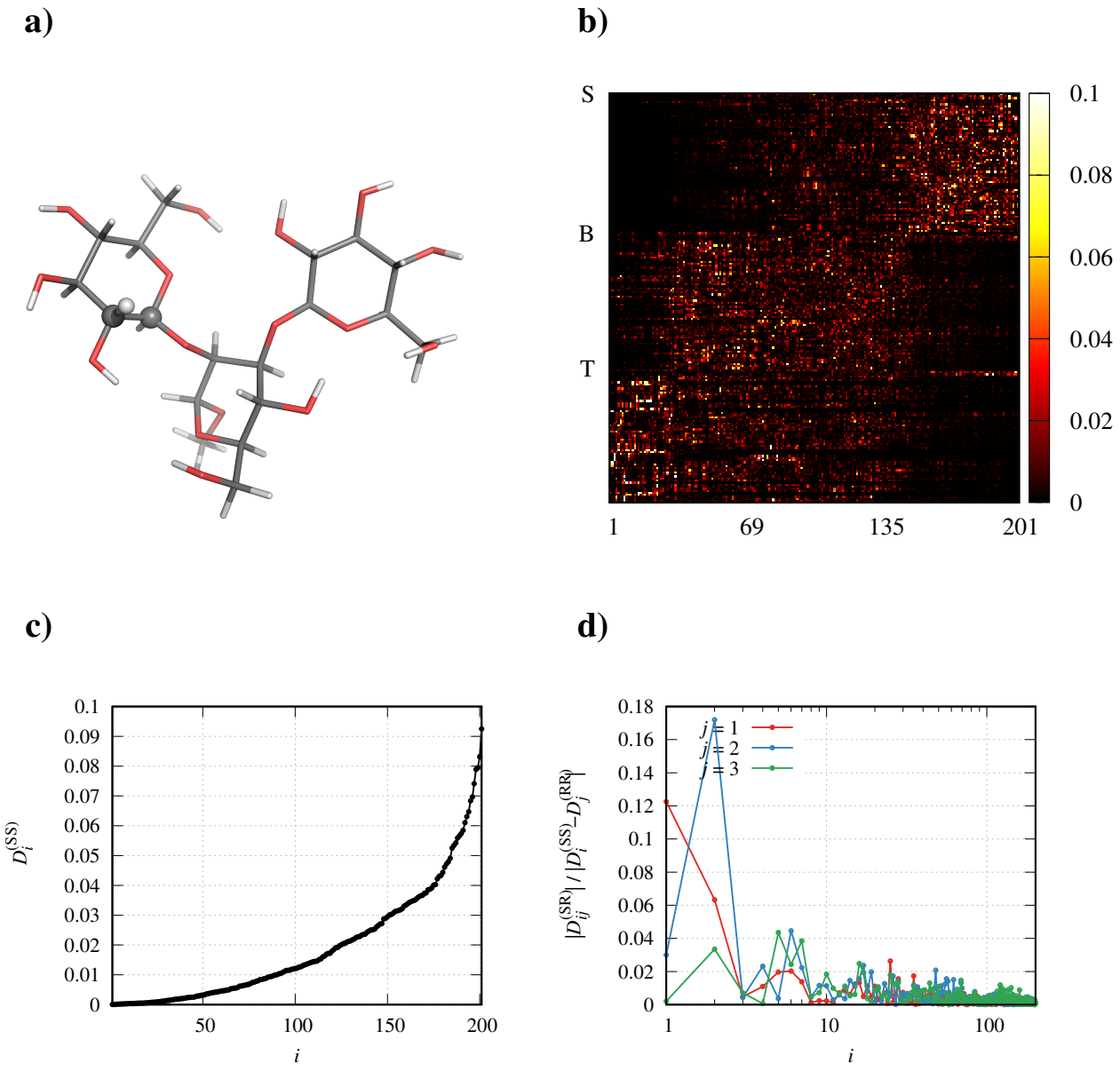

Fig. 3 a) Molecular structure of GGM. b) Color plot of the elements T_{ij}^2 of the matrix diagonalizing the internal block (SS) of the diffusion matrix. The initial row of the stretchings block (rows 1-68), of the bendings block (rows 69-134), and of the torsions block (rows 135-201) is labeled with 'S', 'B', and 'T', respectively. c) Elements $D_i^{(SS)}$ (in fs^{-1}), i.e. eigenvalues of the internal block (SS) of the diffusion matrix. d) Extent of the coupling between the internal motions (each described by the i the normal mode) and the overall rotation (note that the abscissa is in logarithmic scale).

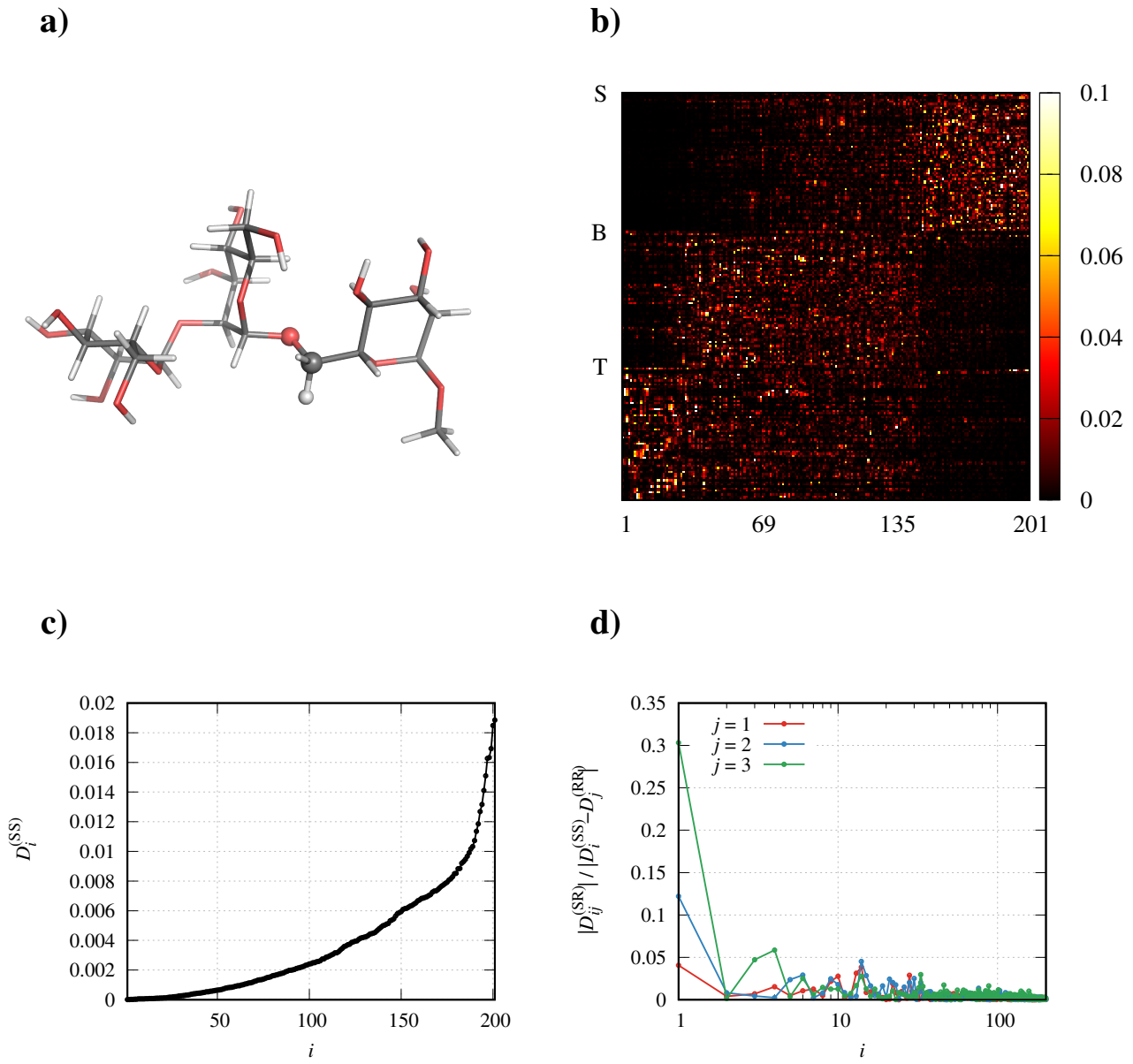

Fig. 4 a) Molecular structure of TRI. b) Color plot of the elements T_{ij}^2 of the matrix diagonalizing the internal block (SS) of the diffusion matrix. The initial row of the stretchings block (rows 1-68), of the bendings block (rows 69-134), and of the torsions block (rows 135-201) is labeled with 'S', 'B', and 'T', respectively. c) Elements $D_i^{(SS)}$ (in fs^{-1}), i.e. eigenvalues of the internal block (SS) of the diffusion matrix. d) Extent of the coupling between the internal motions (each described by the i the normal mode) and the overall rotation (note that the abscissa is in logarithmic scale).

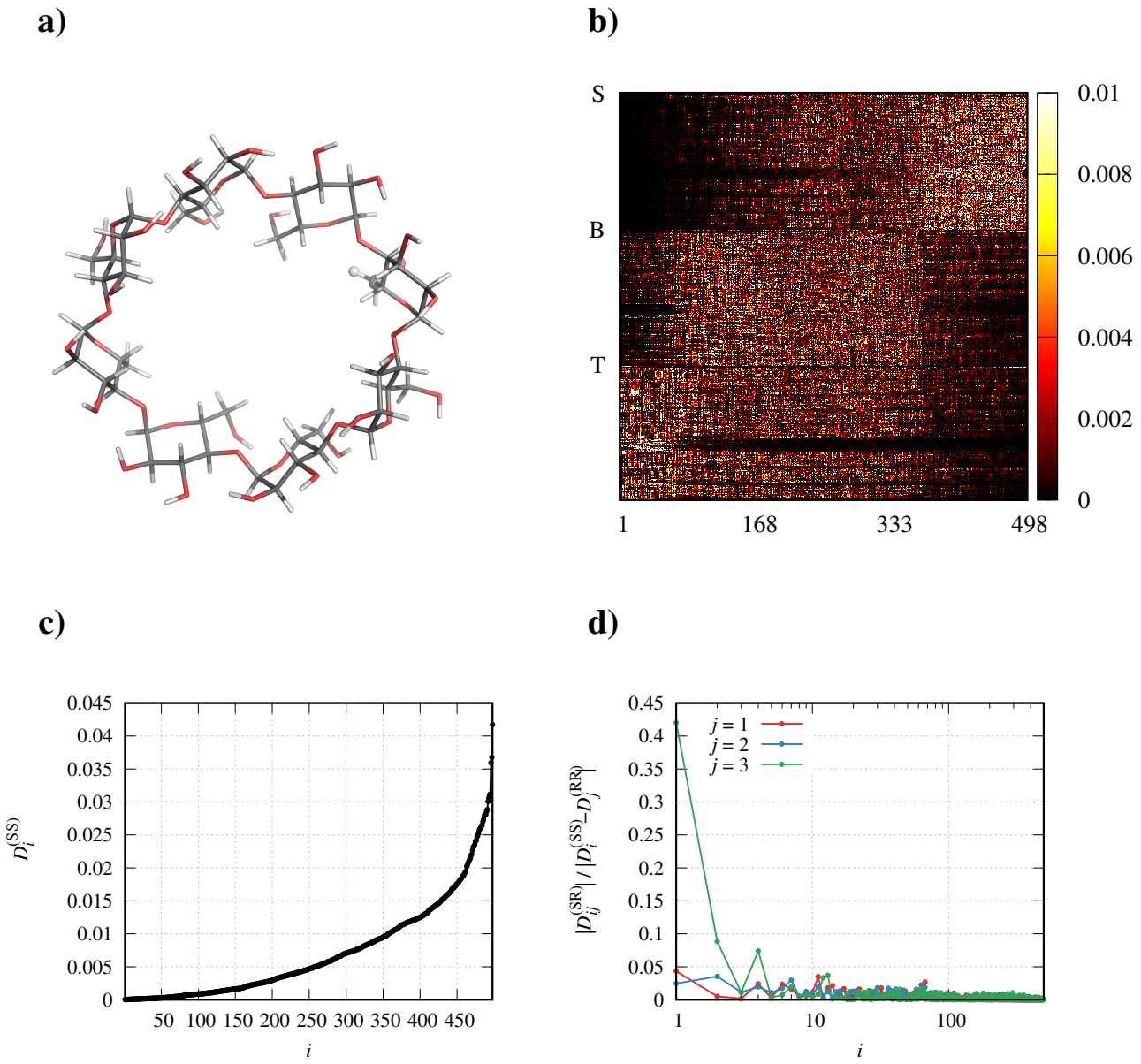

Fig. 5 a) Molecular structure of GCY. b) Color plot of the elements T_{ij}^2 of the matrix diagonalizing the internal block (SS) of the diffusion matrix. The initial row of the stretchings block (rows 1-167), of the bendings block (rows 168-332), and of the torsions block (rows 333-498) is labeled with 'S', 'B', and 'T', respectively. c) Elements $D_i^{(SS)}$ (in fs^{-1}), i.e. eigenvalues of the internal block (SS) of the diffusion matrix. d) Extent of the coupling between the internal motions (each described by the i the normal mode) and the overall rotation (note that the abscissa is in logarithmic scale).

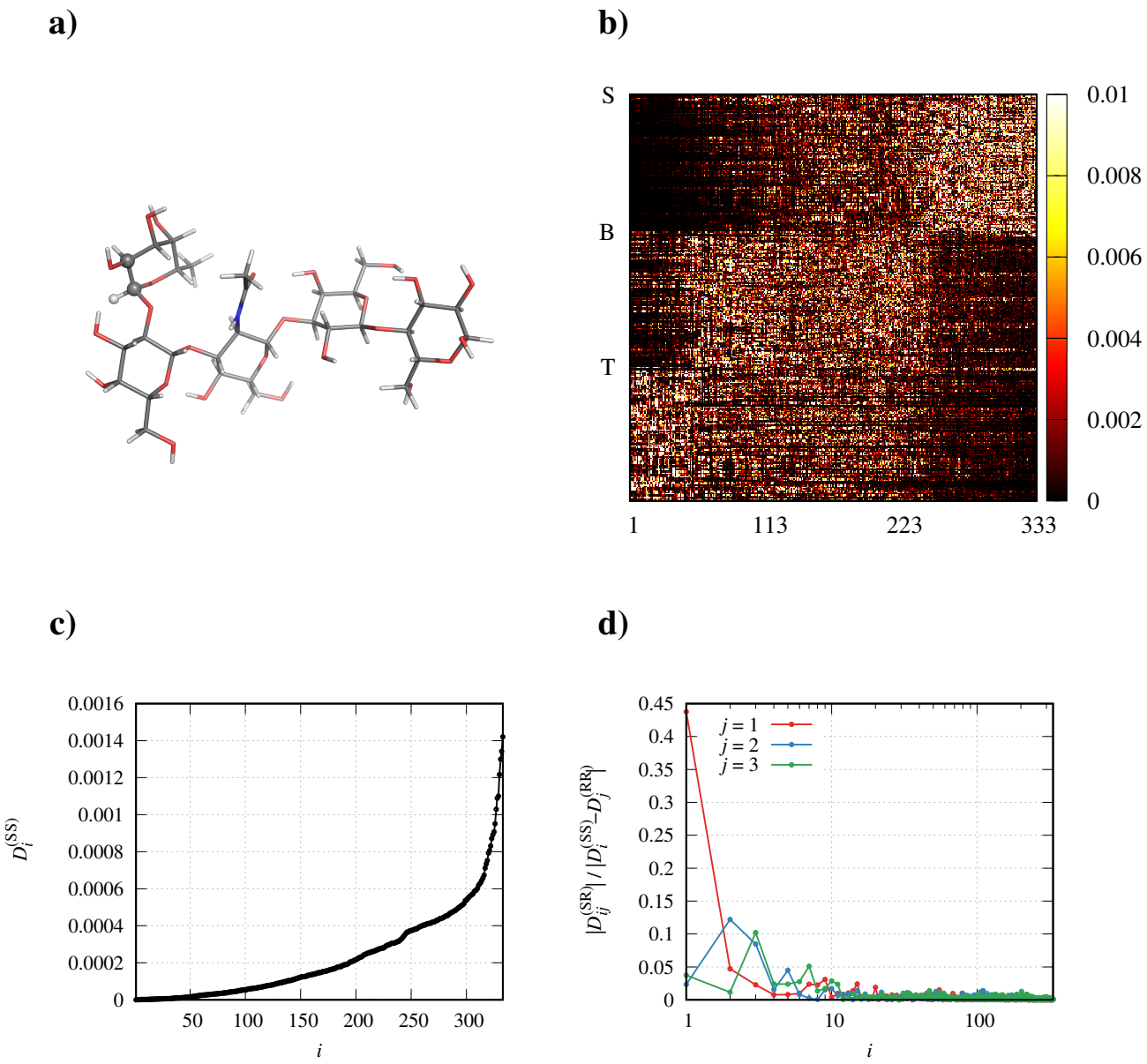

Fig. 6 a) Molecular structure of LNF ($T = 253.0$ K, $\eta = 28.2$ cP). b) Color plot of the elements T^2_{ij} of the matrix diagonalizing the internal block (SS) of the diffusion matrix. The initial row of the stretchings block (rows 1-112), of the bendings block (rows 113-222), and of the torsions block (rows 223-333) is labeled with 'S', 'B', and 'T', respectively. c) Elements $D_i^{(SS)}$ (in fs^{-1}), i.e. eigenvalues of the internal block (SS) of the diffusion matrix. d) Extent of the coupling between the internal motions (each described by the i the normal mode) and the overall rotation (note that the abscissa is in logarithmic scale).

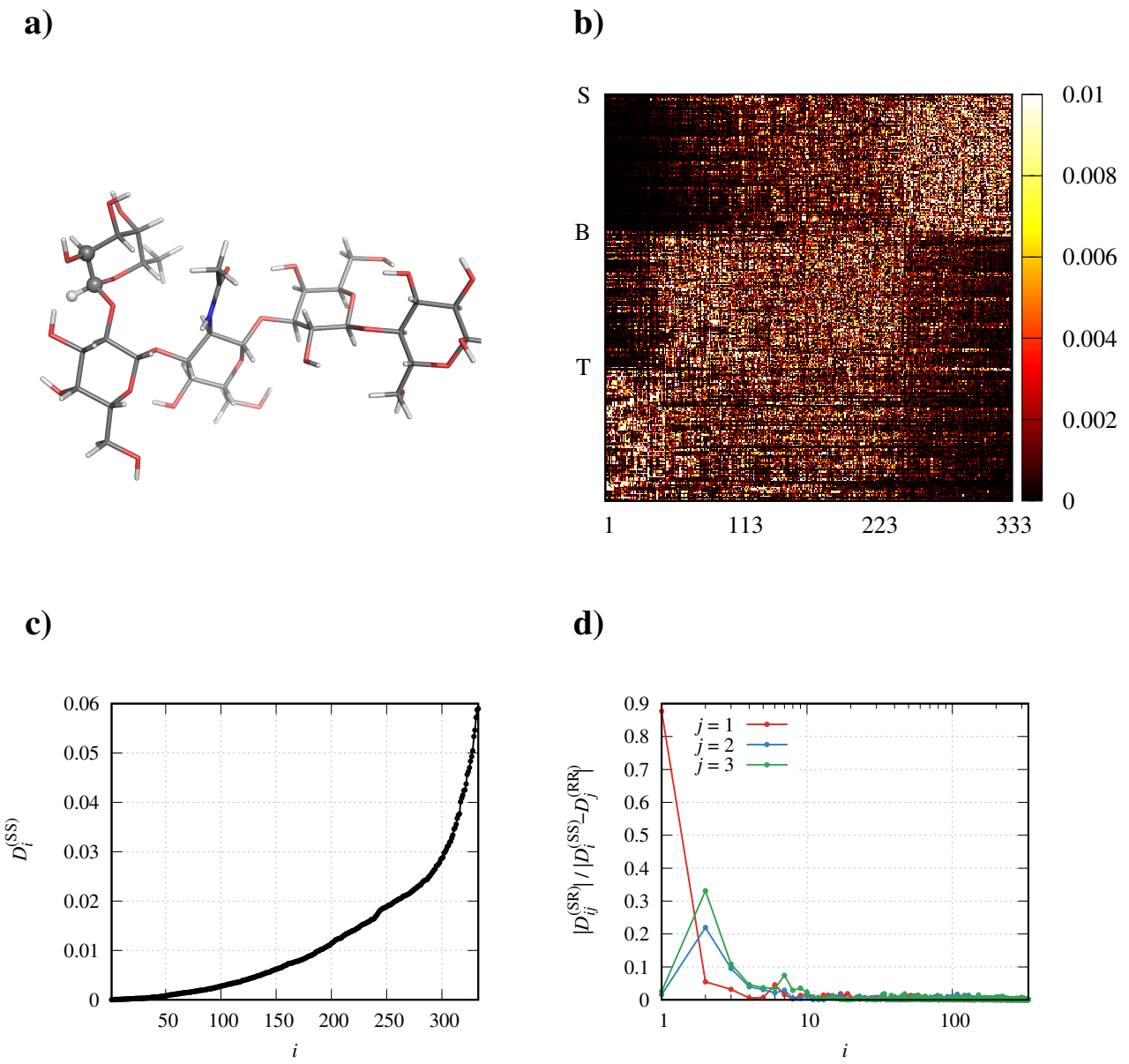

Fig. 7 a) Molecular structure of LNF ($R_{\text{eff}} = 2.0$ Å). b) Color plot of the elements T_{ij}^2 of the matrix diagonalizing the internal block (SS) of the diffusion matrix. The initial row of the stretchings block (rows 1-112), of the bendings block (rows 113-222), and of the torsions block (rows 223-333) is labeled with 'S', 'B', and 'T', respectively. c) Elements $D_i^{(\text{SS})}$ (in fs^{-1}), i.e. eigenvalues of the internal block (SS) of the diffusion matrix. d) Extent of the coupling between the internal motions (each described by the i the normal mode) and the overall rotation (note that the abscissa is in logarithmic scale).

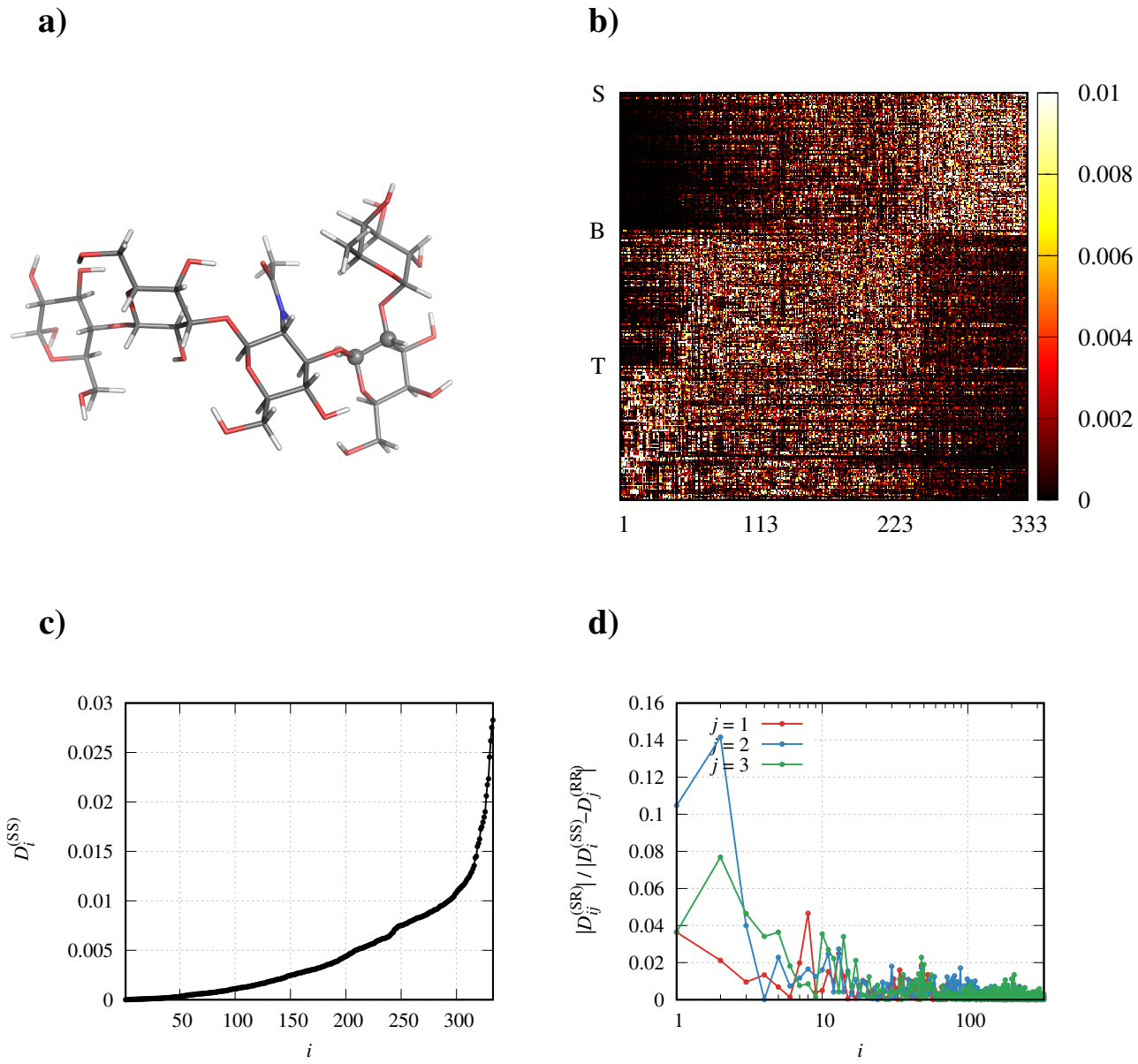

Fig. 8 a) Molecular structure of LNF (triplet in residue B (residue labels as in Fig. 5 of the article)). b) Color plot of the elements T_{ij}^2 of the matrix diagonalizing the internal block (SS) of the diffusion matrix. The initial row of the stretchings block (rows 1-112), of the bendings block (rows 113-222), and of the torsions block (rows 223-333) is labeled with 'S', 'B', and 'T', respectively. c) Elements $D_i^{(SS)}$ (in fs^{-1}), i.e. eigenvalues of the internal block (SS) of the diffusion matrix. d) Extent of the coupling between the internal motions (each described by the i the normal mode) and the overall rotation (note that the abscissa is in logarithmic scale).

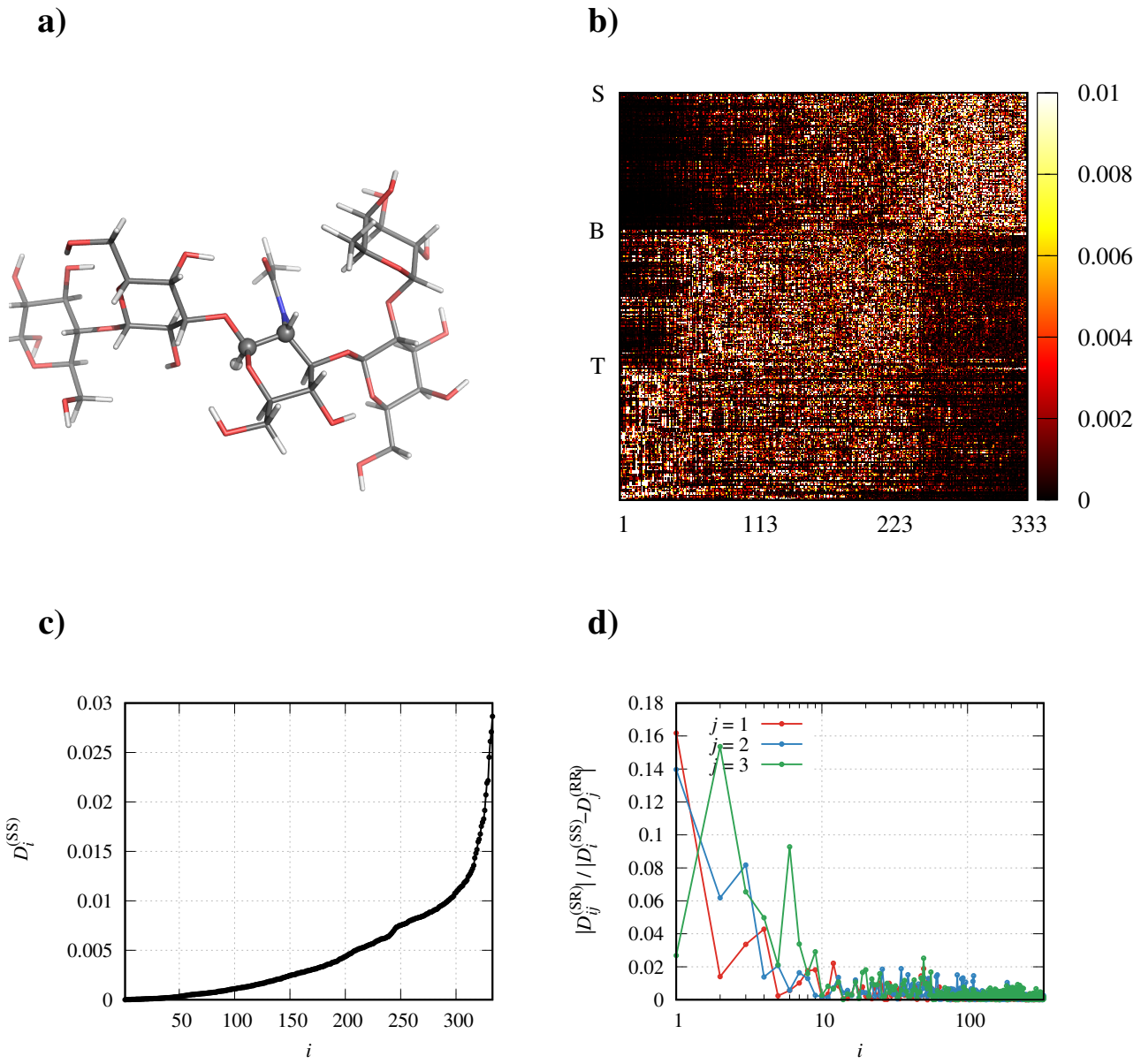

Fig. 9 a) Molecular structure of LNF (triplet in residue C (residue labels as in Fig. 5 of the article)). b) Color plot of the elements T_{ij}^2 of the matrix diagonalizing the internal block (SS) of the diffusion matrix. The initial row of the stretchings block (rows 1-112), of the bendings block (rows 113-222), and of the torsions block (rows 223-333) is labeled with 'S', 'B', and 'T', respectively. c) Elements $D_i^{(SS)}$ (in fs^{-1}), i.e. eigenvalues of the internal block (SS) of the diffusion matrix. d) Extent of the coupling between the internal motions (each described by the i the normal mode) and the overall rotation (note that the abscissa is in logarithmic scale).

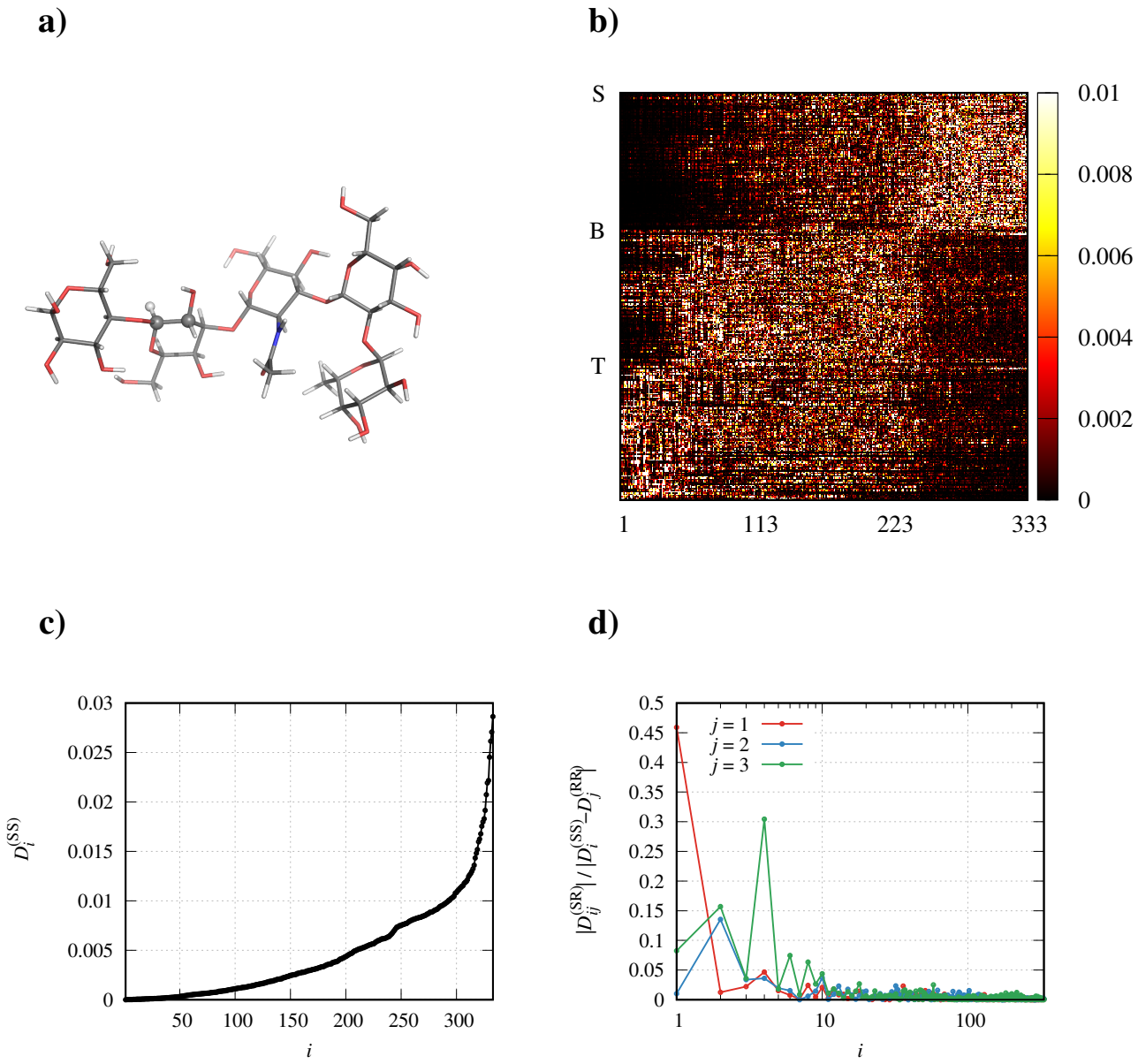

Fig. 10 a) Molecular structure of LNF (triplet in residue D (residue labels as in Fig. 5 of the article)). b) Color plot of the elements T_{ij}^2 of the matrix diagonalizing the internal block (SS) of the diffusion matrix. The initial row of the stretchings block (rows 1-112), of the bendings block (rows 113-222), and of the torsions block (rows 223-333) is labeled with 'S', 'B', and 'T', respectively. c) Elements $D_i^{(SS)}$ (in fs^{-1}), i.e. eigenvalues of the internal block (SS) of the diffusion matrix. d) Extent of the coupling between the internal motions (each described by the i the normal mode) and the overall rotation (note that the abscissa is in logarithmic scale).

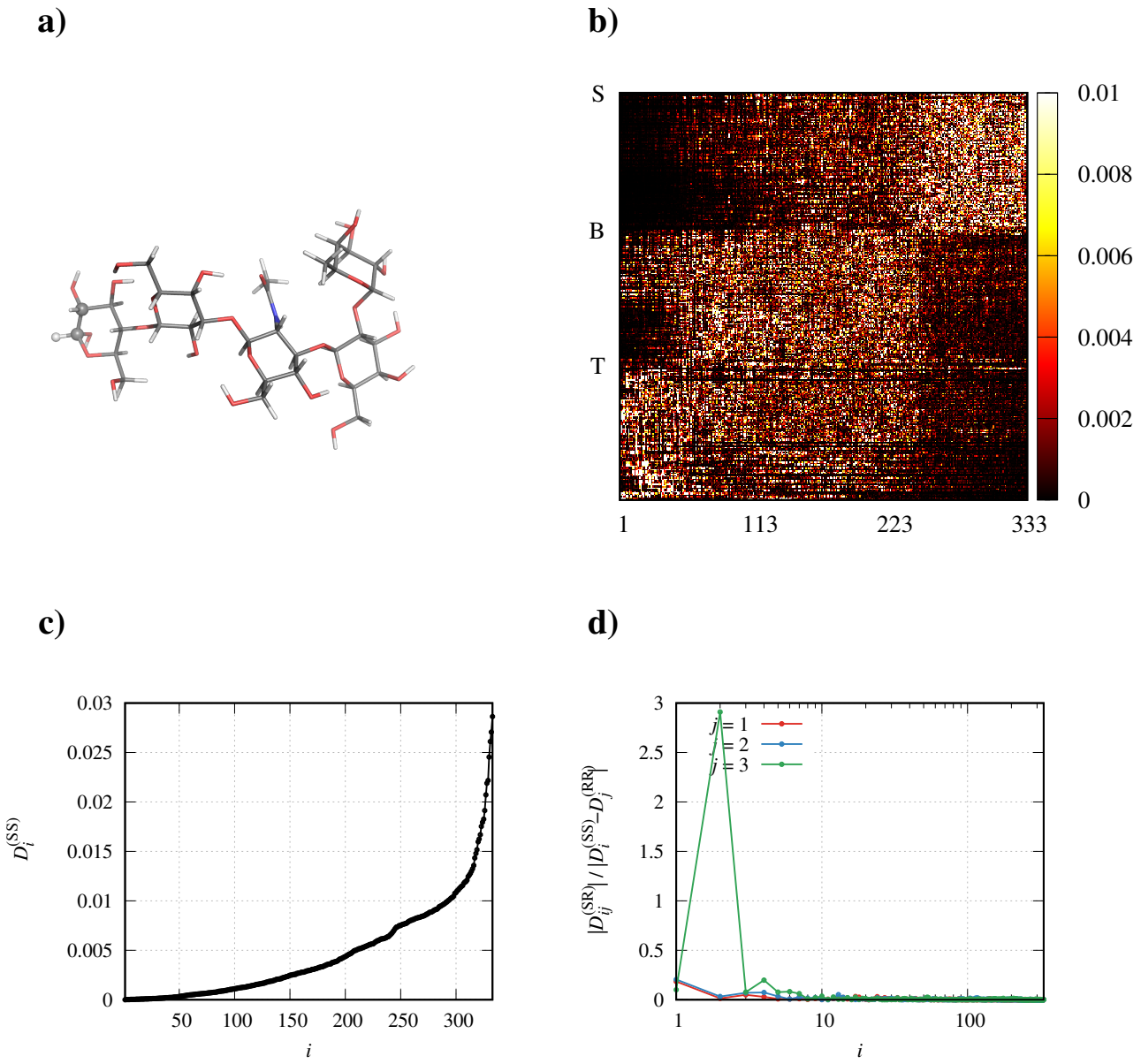

Fig. 11 a) Molecular structure of LNF (triplet in residue E (residue labels as in Fig. 5 of the article)). b) Color plot of the elements T_{ij}^2 of the matrix diagonalizing the internal block (SS) of the diffusion matrix. The initial row of the stretchings block (rows 1-112), of the bendings block (rows 113-222), and of the torsions block (rows 223-333) is labeled with 'S', 'B', and 'T', respectively. c) Elements $D_i^{(SS)}$ (in fs^{-1}), i.e. eigenvalues of the internal block (SS) of the diffusion matrix. d) Extent of the coupling between the internal motions (each described by the i the normal mode) and the overall rotation (note that the abscissa is in logarithmic scale).

	$i=1$	$i=2$	$i=3$
LNF ($T=253.0$ K, $\eta=28.2$ cP)			
$D_i^{(\mathrm{RR})}$	1.67×10^{-7}	3.26×10^{-7}	5.05×10^{-7}
$(\mathrm{egv}[\mathbf{D}])_i$	5.83×10^{-9}	6.09×10^{-9}	9.28×10^{-9}
LNF ($R_{\mathrm{eff}}=2.0$ Å)			
$D_i^{(\mathrm{RR})}$	1.03×10^{-5}	2.01×10^{-5}	3.12×10^{-5}
$(\mathrm{egv}[\mathbf{D}])_i$	2.07×10^{-7}	2.15×10^{-7}	3.61×10^{-7}
LNF (probe: ^{13}CH on C-1 of residue B)			
$D_i^{(\mathrm{RR})}$	3.97×10^{-6}	7.87×10^{-6}	1.29×10^{-5}
$(\mathrm{egv}[\mathbf{D}])_i$	1.41×10^{-7}	1.47×10^{-7}	2.27×10^{-7}
LNF (probe: ^{13}CH on C-1 of residue C)			
$D_i^{(\mathrm{RR})}$	3.99×10^{-6}	7.89×10^{-6}	1.27×10^{-5}
$(\mathrm{egv}[\mathbf{D}])_i$	1.41×10^{-7}	1.48×10^{-7}	2.24×10^{-7}
LNF (probe: ^{13}CH on C-1 of residue D)			
$D_i^{(\mathrm{RR})}$	3.97×10^{-6}	7.87×10^{-6}	1.28×10^{-5}
$(\mathrm{egv}[\mathbf{D}])_i$	1.41×10^{-7}	1.47×10^{-7}	2.19×10^{-7}
LNF (probe: ^{13}CH on C-1 of residue E)			
$D_i^{(\mathrm{RR})}$	4.02×10^{-6}	7.85×10^{-6}	1.23×10^{-5}
$(\mathrm{egv}[\mathbf{D}])_i$	1.41×10^{-7}	1.46×10^{-7}	2.22×10^{-7}

Table 1 Elements of the diagonal rotational block $\mathbf{D}^{(\mathrm{RR})}$ of the roto-conformational diffusion tensor $\mathbf{D}$ and first three of eigenvalues of the roto-conformational diffusion tensor $\mathbf{D}$ for the LNF system calculated using the same parameters as in Figs. 6-11 of the ESI. Units are fs^{-1}.

3 Fokker-Planck equation in internal coordinates

Table 2 Table of symbols

Symbol	Meaning
Ω_μ	Euler angles of the μ interaction frame μF with respect to the LF
Ω	Euler angles of the MF with respect to the LF
$\overline{\Omega}_\mu$	Euler angle of μF with respect to the MF
$n, N = 3n-6$	number of atoms, number of internal coordinates
H, K, U	total energy, kinetic energy, potential energy
$\mathbf{L}$	angular momentum
q^μ	μ-th internal variable
p_μ	μ-th conjugate momentum
$\mathbf{I}$	inertia tensor
$\mathbf{A}_\mu$	gauge potential
$g^{\mu\nu}$	contravariant metric tensor components
$\mathbf{x}$	configuration phase space $\mathbf{\Omega}, \mathbf{q}$
$\boldsymbol{\pi}$	phase space of momenta $\mathbf{L}, \mathbf{p}$
$\mathcal{Q}$	phase space
$\rho(\mathcal{Q}, t)$	conditional probability
Γ	Fokker-Planck time evolution operator for $\rho(\mathcal{Q}, t)$
$\rho(\mathcal{Q})$	equilibrium distribution
$\boldsymbol{\xi}$	friction tensor
$\langle \ldots \rangle_\alpha$	integration over coordinate α

We sketch some of the conclusions previously reported in refs. 8 and 9, to which the reader is referred for a detailed and rigorous complete exposition. Our starting point is given by a simplified version of Eqns. (34-39) of reference 8. The definition of the symbols used for the main variables and parameters are summarized in Table 2. We make the following hypotheses. First, the molecule, made of n atoms, is described by a conditional probability $\rho(\mathcal{Q}, t)$ where $\mathcal{Q}$ are a set of coordinates and momenta $\mathcal{Q} = (\Omega, \mathbf{q}; \mathbf{L}, \mathbf{p}) = (\mathbf{x}, \boldsymbol{\pi})$: Ω are a set of orientation coordinates (e.g Euler angles) specifying the instantaneous orientation of a generic molecule-fixed frame (MF) with respect to the laboratory or inertial frame (LF), $\mathbf{L}$ is the related angular momentum; $\mathbf{q}$ is the collection $N = 3n-6$ of internal coordinates specifying its shape, $\mathbf{p}$ is the related set of conjugate momenta; $\mathbf{x}$ is the collection of positions and $\boldsymbol{\pi}$ of momenta. Second, the specific definitions of the MF, i.e. of Ω and $\mathbf{q}$ as functions of the native Cartesian coordinates can be arbitrarily chosen, provided that proper invariance conditions are considered[10]. A possible choice is for instance given by Casimir-Eckart conditions[11], or

simply based on the instantaneous position of three (non collinear) atoms. Here we shall only assume that these functions are known and computable. Finally, we neglect center-of-mass coordinates and momenta from our description. This is acceptable for a molecule in a isotropic medium, for which only rotation-dependent correlation functions are considered. The time evolution equation for $\rho(\mathcal{Q},t)$ is given by[8,12]

$$\begin{aligned} \frac{\partial \rho(\mathcal{Q},t)}{\partial t} &= -\hat{\Gamma}\rho(\mathcal{Q},t) \\ \hat{\Gamma} &= \hat{\mathrm{Pr}} - \hat{\nabla}^{\mathrm{tr}}_{\mathcal{Q}}\mathbf{J}\rho(\mathcal{Q})\hat{\nabla}_{\mathcal{Q}}\rho(\mathcal{Q})^{-1} \end{aligned} \tag{1}$$

here $\hat{\nabla}_{\mathcal{Q}}$ is defined as $(\hat{\mathbf{M}},\hat{\nabla}_{\mathbf{L}},\hat{\nabla}_{\mathbf{q}},\hat{\nabla}_{\mathbf{p}})^{\mathrm{tr}}$, where $\hat{\mathbf{M}}$ is the generator of infinitesimal rotations for a rigid body, acting on Ω; $2(N+3)\times 2(N+3)$ matrix $\mathbf{J}$ is

$$\mathbf{J} = k_B T \begin{pmatrix} \mathbf{0} & -\mathbf{1} \\ \mathbf{1} & \boldsymbol{\xi} \end{pmatrix} \tag{2}$$

$\boldsymbol{\xi}$ is the friction tensor, which in general depends upon $\mathbf{q}$:

$$\boldsymbol{\xi} = \begin{pmatrix} \boldsymbol{\xi}_{\mathrm{RR}} & \boldsymbol{\xi}_{\mathrm{RS}} \\ \boldsymbol{\xi}_{\mathrm{SR}} & \boldsymbol{\xi}_{\mathrm{SS}} \end{pmatrix} \tag{3}$$

The precessional operator is $\hat{\mathrm{Pr}} = \mathbf{L}^{\mathrm{tr}}\left(\hat{\nabla}_{\mathbf{L}}H \times \hat{\nabla}_{\mathbf{L}}\right)$. Hydrodynamic models[13,14] can be employed to evaluate approximately $\boldsymbol{\xi}_{\mathrm{AB}}$, and we shall assume here they are valid.[8,13,14]. Finally, the equilibrium distribution $\rho(\mathcal{Q})$ is defined with respect to the total energy H

$$\rho(\mathcal{Q}) = \exp(-H[\mathcal{Q}]/k_B T)/\langle \exp(-H(\mathcal{Q})/k_B T)\rangle \tag{4}$$

where the average $\langle \ldots \rangle$ is defined with respect to $\mathcal{Q}$, and the total free energy H is

$$H = K + U = \frac{1}{2}\mathbf{L}^{\mathrm{tr}}\mathbf{I}^{-1}\mathbf{L} + \frac{1}{2}g^{\mu\nu}(p_\mu - \mathbf{L}^{\mathrm{tr}}\mathbf{A}_\mu)(p_\nu - \mathbf{L}^{\mathrm{tr}}\mathbf{A}_\nu) + U \tag{5}$$

here $g^{\mu\nu}$ is the contravariant metric tensor, A_μ is the gauge potential, $\mathbf{I}$ is the inertia tensor, U is the internal energy, depending upon $\mathbf{q}$.

4 Projection of the momenta

We define

$$\begin{aligned}\rho(\mathbf{x}) &= \int dp\rho(\mathcal{Q}) = \langle\rho(\mathcal{Q})\rangle_{\boldsymbol{\pi}} = \exp(-U/k_BT)/\langle\exp(-U/k_BT)\rangle_{\mathbf{x}} \\ \rho(\boldsymbol{\pi}|\mathbf{x}) &= \frac{\rho(\mathcal{Q})}{\rho(\mathbf{x})} \\ \rho(\mathbf{x},t) &= \langle\rho(\mathcal{Q})\rangle_{\boldsymbol{\pi}}\end{aligned} \tag{6}$$

and the symmetrized, for convenience, Fokker-Planck equation

$$\frac{\partial\tilde{\rho}(\mathcal{Q},t)}{\partial t} = -\tilde{\Gamma}\tilde{\rho}(\mathcal{Q},t) \tag{7}$$

where $\tilde{\rho}(\mathcal{Q},t) = \rho(\mathcal{Q},t)\rho(\mathcal{Q})^{-1/2}$, $\tilde{\Gamma} = \rho(\mathcal{Q})^{-1/2}\hat{\Gamma}\rho(\mathcal{Q})^{1/2}$. We partition the symmetrized time evolution operator in two parts

$$\begin{aligned}\tilde{\Gamma}_{\text{int}} = \hat{\text{Pr}} + k_BT\rho(\boldsymbol{\pi}|\mathbf{x})^{-1/2}\Big[&\rho(x)^{-1/2}\hat{\nabla}^{\text{tr}}_{\mathbf{x}}\rho(\mathbf{x})^{1/2}\rho(\boldsymbol{\pi}|\mathbf{x})\hat{\nabla}_{\boldsymbol{\pi}} \\ &-\hat{\nabla}^{\text{tr}}_{\boldsymbol{\pi}}\rho(\boldsymbol{\pi}|\mathbf{x})\rho(\mathbf{x})^{1/2}\hat{\nabla}_{\mathbf{x}}\rho(x)^{-1/2}\Big]\rho(\boldsymbol{\pi}|\mathbf{x})^{-1/2}\end{aligned} \tag{8}$$

Notice that the total energy can be written in general in the form

$$H = K + U = \frac{1}{2}p^{\text{tr}}\mathbf{M}(\mathbf{x})p + U(\mathbf{x}) \tag{9}$$

where $\mathbf{M}$ is symmetric.

Using a bra-ket notation, we define $|0\rangle_{\boldsymbol{\pi}} = \rho(\boldsymbol{\pi}|\mathbf{x})^{1/2}$ and we define the projection operator

$$\hat{P} = |0\rangle_{\boldsymbol{\pi}}\langle 0| \tag{10}$$

One shows easily that for two generic functions $f(\mathbf{x}), g(\mathcal{Q})$

$$\begin{aligned}\tilde{\Gamma}_0|0\rangle_{\boldsymbol{\pi}}f(\mathbf{x}) &= 0 \\ \hat{P}\tilde{\Gamma}_0 g(\mathcal{Q}) &= 0\end{aligned} \tag{11}$$

We assume that $\mathbf{x}$ and $\boldsymbol{\pi}$ are initially statistically uncorrelated, so that the initial phase density is $\rho(\mathcal{Q},0) = |0\rangle_{\boldsymbol{\pi}}\rho(\mathbf{x},0)$. Defining $\hat{Q} = 1 - \hat{P}$, the well-known formal solution is obtained (see I):

$$\begin{aligned}\frac{\partial \hat{P}\tilde{\rho}(\mathcal{Q},t)}{\partial t} &= -\hat{P}\tilde{\Gamma}\hat{P}\tilde{\rho}(\mathcal{Q},t) + \\ &+ \int_0^t d\tau \hat{P}\tilde{\Gamma}\exp(-\hat{Q}\tilde{\Gamma}\tau)\hat{Q}\tilde{\Gamma}\hat{P}\tilde{\rho}(\mathcal{Q},t-\tau) + \\ &+ \hat{P}\tilde{\Gamma}\exp(-\hat{Q}\tilde{\Gamma}t)\hat{Q}\tilde{\rho}(\mathcal{Q},0) \end{aligned} \tag{12}$$

The first term is the zero-order averaged operator, the second and most complex term is defined in terms of a general kernel that is a function of time. The latter goes to zero, due to the initial conditions assumed. One finds:

$$\begin{aligned}\frac{\partial \tilde{\rho}(\mathbf{x},t)}{\partial t} &= -\langle 0|\tilde{\Gamma}_{\text{int}}|0\rangle_{\boldsymbol{\pi}}\tilde{\rho}(\mathbf{x},t) + \\ &+ \int_0^t \langle 0|\tilde{\Gamma}_{\text{int}}\exp\left(-\hat{Q}\tilde{\Gamma}\tau\right)\hat{Q}\tilde{\Gamma}_{\text{int}}|0\rangle_{\boldsymbol{\pi}}\tilde{\rho}(\mathbf{x},t-\tau)d\tau \end{aligned} \tag{13}$$

where $\tilde{\rho}(\mathbf{x},t) = \rho(\mathbf{x},t)\rho(\mathbf{x})^{-1/2}$. The Fourier-Laplace transform of Eq. (13) yields

$$\tilde{\rho}(\mathbf{x},\omega) = \left[i\omega + \langle 0|\tilde{\Gamma}_{\text{int}}|0\rangle_{\boldsymbol{\pi}} - \langle 0|\tilde{\Gamma}_{\text{int}}\left(i\omega + \hat{Q}\tilde{\Gamma}\right)^{-1}\hat{Q}\tilde{\Gamma}_{\text{int}}|0\rangle_{\boldsymbol{\pi}}\right]^{-1}\tilde{\rho}(\mathbf{x},0) \tag{14}$$

The symmetrized form of a generic correlation function for observables depending only upon x is

$$G(t) = \langle f(\mathbf{x})\rho^{1/2}(\mathcal{Q})|\exp\left(-\tilde{\Gamma}t\right)|g(\mathbf{x})\rho^{1/2}(\mathcal{Q})\rangle = \langle f(\mathbf{x})\rho^{1/2}(\mathcal{Q})|\tilde{\rho}(\mathcal{Q},t)\rangle \tag{15}$$

where $\tilde{\rho}(\mathcal{Q},t)$ is the symmetrized density evolved from the initial $\tilde{\rho}(\mathcal{Q},0) = g(\mathbf{x})\rho^{1/2}(\mathcal{Q})$. The Fourier-Laplace transform of $G(t)$ is

$$\begin{aligned} J(i\omega) &= \langle f(\mathbf{x})\tilde{\rho}^{1/2}(\mathcal{Q})|\left(i\omega + \tilde{\Gamma}\right)^{-1}|g(\mathbf{x})\rho^{1/2}(\mathcal{Q})\rangle = \\ &= \langle f(\mathbf{x})\rho^{1/2}(x)|\tilde{\rho}(\mathbf{x},\omega)\rangle_{\mathbf{x}} = \\ &= \langle f(\mathbf{x})\left[i\omega + \hat{G}(\omega)^{-1}\right]\rho^{1/2}(\mathbf{x})\rangle_{\mathbf{x}} \end{aligned} \tag{16}$$

where

$$\hat{G}(\omega) = \langle 0|\tilde{\Gamma}_{\rm int}|0\rangle_{\boldsymbol{\pi}} - \langle 0|\tilde{\Gamma}_{\rm int}\left(i\omega + \tilde{Q}\tilde{\Gamma}\right)^{-1}\tilde{Q}\tilde{\Gamma}_{\rm int}|0\rangle_{\boldsymbol{\pi}} \tag{17}$$

To treat in practice Eq. (16) we follow a standard route. We start with the Dyson identity, valid for any two generic operators $\hat{A}$, $\hat{B}$:

$$\left(\hat{A}+\hat{B}\right)^{-1} = \hat{A}^{-1}\left[1 - \hat{B}\left(\hat{A}+\hat{B}\right)^{-1}\right] \tag{18}$$

which can be easily proved by inspection. We apply now the identity to $\left(i\omega + \tilde{Q}\tilde{\Gamma}\right)^{-1}$

$$\begin{aligned}\left(i\omega + \tilde{Q}\tilde{\Gamma}\right)^{-1} &= \left(i\omega + \tilde{\Gamma}_0 + \tilde{Q}\tilde{\Gamma}_{\rm int}\right)^{-1} \\ &= \left(i\omega + \tilde{\Gamma}_0\right)^{-1}\left[1 - \tilde{Q}\tilde{\Gamma}_{\rm int}\left(i\omega + \tilde{\Gamma}_0 + \tilde{Q}\tilde{\Gamma}_{\rm int}\right)^{-1}\right]\end{aligned} \tag{19}$$

Finally $\left(i\omega + \tilde{Q}\tilde{\Gamma}\right)^{-1}$ takes the more convenient form

$$\begin{aligned}\left(i\omega + \tilde{Q}\tilde{\Gamma}\right)^{-1} &= \left[1 + \left(i\omega + \tilde{\Gamma}_0\right)^{-1}\tilde{Q}\tilde{\Gamma}_{\rm int}\right]^{-1}\left(i\omega + \tilde{\Gamma}_0\right)^{-1} \\ &= \sum_{k=0}^{\infty}(-1)^k\left[\left(i\omega + \tilde{\Gamma}_0\right)^{-1}\tilde{Q}\tilde{\Gamma}_{\rm int}\right]^k\left(i\omega + \tilde{\Gamma}_0\right)^{-1}\end{aligned} \tag{20}$$

Substituting in Eq. 16 and rearranging terms one gets

$$\hat{G}(\omega) = \sum_{k=0}^{\infty}(-1)^k\langle 0|\tilde{\Gamma}_{\rm int}\left[\left(i\omega + \tilde{\Gamma}_0\right)^{-1}\tilde{Q}\tilde{\Gamma}_{\rm int}\right]^k|0\rangle_{\boldsymbol{\pi}} = \sum_{k=0}^{\infty}\hat{g}_k(\omega) \tag{21}$$

this is essentially a perturbation expansion where the k-th term $\hat{G}_k(\omega)$ is of order $k+1$ in $\tilde{\Gamma}_{\rm int}$. Formally, this expression is equivalent to a total time ordered cumulant (TTOC) expansion. The diffusive limit is obtained by arresting the expansion to $k=1$, and neglecting the residual

dependence at short time The first term ($k=0$) can be shown to be zero, i.e.

$$\begin{aligned}\langle 0|\tilde{\Gamma}_{\text{int}}|0\rangle_{\boldsymbol{\pi}} &= \langle 0|\hat{\text{Pr}}|0\rangle_{\boldsymbol{\pi}} + \\ &+k_BT\left[\rho(\mathbf{x})^{-1/2}\hat{\nabla}^{\text{tr}}_{\mathbf{x}}\rho(\mathbf{x})^{1/2}\langle\rho(\boldsymbol{\pi}|\mathbf{x})\hat{\nabla}_{\boldsymbol{\pi}}\rangle_{\boldsymbol{\pi}}+\right. \\ &\left.-\langle\hat{\nabla}^{\text{tr}}_{\boldsymbol{\pi}}\rho(\boldsymbol{\pi}|\mathbf{x})\rangle\rho(\mathbf{x})^{1/2}\hat{\nabla}_{\mathbf{x}}\rho(\mathbf{x})^{-1/2}\right]=0\end{aligned} \tag{22}$$

The second term is slightly more involved. After some passages, one obtains

$$\langle 0|\tilde{\Gamma}_{\text{int}}\left(i\omega+\tilde{\Gamma}\right)^{-1}\tilde{\Gamma}|0\rangle_{\boldsymbol{\pi}}=\rho(\mathbf{x})^{-1/2}\hat{\nabla}^{\text{tr}}_{\mathbf{x}}\mathbf{D}(\omega)\rho(\mathbf{x})\hat{\nabla}_{\mathbf{x}}\rho(\mathbf{x})^{-1/2} \tag{23}$$

where $\mathbf{D}(\omega)$ is

$$\mathbf{D}(\omega,\mathbf{q})=\mathbf{M}^{-1}\langle\boldsymbol{\pi}\rho(\boldsymbol{\pi}|\mathbf{x})^{1/2}|(i\omega+\tilde{\Gamma})^{-1}|\boldsymbol{\pi}^{\text{tr}}\rho(\boldsymbol{\pi}|\mathbf{x})^{1/2}\rangle_{\boldsymbol{\pi}}\mathbf{M}^{-1} \tag{24}$$

for $\omega\to 0$, given the structure of $\tilde{\Gamma}_0$ one gets exactly

$$\mathbf{D}=\mathbf{M}^{-1}\langle\boldsymbol{\pi}\boldsymbol{\pi}^{\text{tr}}\rho(\boldsymbol{\pi}|\mathbf{x})\rangle_{\boldsymbol{\pi}}\boldsymbol{\xi}(x)^{-1}=k_BT\boldsymbol{\xi}^{-1} \tag{25}$$

Finally, we can define a symmetrized diffusive (Smoluchowski) equation

$$\begin{aligned}\frac{\partial}{\partial t}\tilde{\rho}(\mathbf{x},t)&=-\tilde{\Gamma}_D\tilde{\rho}(\mathbf{x},t)\\ \tilde{\Gamma}_{\text{D}}&=-\tilde{\rho}(\mathbf{x})^{-1/2}\hat{\nabla}^{\text{tr}}_{\mathbf{x}}\mathbf{D}\tilde{\rho}(\mathbf{x})\hat{\nabla}_{\mathbf{x}}\tilde{\rho}(\mathbf{x})^{-1/2}\end{aligned} \tag{26}$$

which of course is equivalent to the unsymmetrized form previously shown.

Notes and references

1 J. A. Rackers, Z. Wang, C. Lu, M. L. Laury, L. Lagardère, M. J. Schnieders, J.-P. Piquemal, P. Ren and J. W. Ponder, *Journal of Chemical Theory and Computation*, 2018, **14**, 5273–5289.

2 N. L. Allinger, Y. H. Yuh and J. H. Lii, *Journal of the American Chemical Society*, 1989, **111**, 8551–8566.

3 J. H. Lii and N. L. Allinger, *Journal of the American Chemical Society*, 1989, **111**, 8566–8575.

4 J. H. Lii and N. L. Allinger, *Journal of the American Chemical Society*, 1989, **111**, 8576–8582.

5 V. Stroylov, M. Panova and P. Toukach, *International Journal of Molecular Sciences*, 2020, **21**, 7626.

6 B. L. Foley, M. B. Tessier and R. J. Woods, *WIREs Computational Molecular Science*, 2012, **2**, 652–697.

7 A. D. J. MacKerell, D. Bashford, M. Bellott, R. L. J. Dunbrack, J. D. Evanseck, M. J. Field, S. Fischer, J. Gao, H. Guo, S. Ha, D. Joseph-McCarthy, L. Kuchnir, K. Kuczera, F. T. K. Lau, C. Mattos, S. Michnick, T. Ngo, D. T. Nguyen, B. Prodhom, W. E. Reiher, B. Roux, M. Schlenkrich, J. C. Smith, R. Stote, J. Straub, M. Watanabe, J. Wiórkiewicz-Kuczera, D. Yin and M. Karplus, *The Journal of Physical Chemistry B*, 1998, **102**, 3586–3616.

8 A. Polimeno, M. Zerbetto and D. Abergel, *Journal of Chemical Physics*, 2019, **150**, 184107.

9 A. Polimeno, M. Zerbetto and D. Abergel, *Journal of Chemical Physics*, 2019, **150**, 184108.

10 R. G. Littlejohn and M. Reinsch, *Review of Modern Physics*, 1997, **69**, 213–275.

11 W. D. Allen and A. G. Csaszar, *Journal of Chemical Physics*, 1993, **98**, 2983–3015.

12 J. T. Hynes and J. Deutch, *Physical Chemistry - An Advanced Treatise*, Academic Press, 1975, vol. XIB.

13 J. Rotne and S. Prager, *Journal of Chemical Physics*, 1969, **50**, 4831–4837.

14 V. Barone, M. Zerbetto and A. Polimeno, *Journal of Computational Chemistry*, 2009, **30**, 2–13.